RSC Advances

PAPER

View Article Online
View Journal | View Issue

Cite this: *RSC Adv.*, 2020, **10**, 29868

High-throughput in-focus differential interference contrast imaging of three-dimensional orientations of single gold nanorods coated with a mesoporous silica shell†

Geun Wan Kim,[ab] Seokyoung Yoon,[c] Jung Heon Lee *[cd] and Ji Won Ha *[ab]

Received 28th May 2020
Accepted 2nd August 2020

DOI: 10.1039/d0ra04704j

rsc.li/rsc-advances

Plasmonic gold nanorods (AuNRs) have been widely applied as optical orientation probes in many biophysical studies. However, characterizing the various three-dimensional (3D) orientations of AuNRs in the same focal plane of the objective lens is a challenging task. To overcome this challenge, we fabricated single AuNRs (10 nm × 30 nm) coated with either an elliptical or spherical mesoporous silica shell (AuNRs@mSiO$_2$). Unlike bare AuNRs and elliptical AuNRs@mSiO$_2$, spherical AuNRs@mSiO$_2$ contained randomly oriented AuNR cores in 3D space, which could be observed on the same focal plane within a single frame by differential interference contrast (DIC) microscopy. The spherical AuNRs@mSiO$_2$ thus achieved high-throughput detection. The proposed approach can overcome the limitations of the current gel-matrix method, which requires vertical scanning of the embedded AuNRs to capture different focal planes.

Introduction

Direct visualization and tracking with optical probes at high spatial and temporal resolution can reveal the complex dynamics and interactions in chemical and biological processes.[1–3] By investigating the rotational dynamics of nanoprobes, we can uncover a new dimension of information that is hidden in conventional three-dimensional (3D) single-particle tracking. Recently, plasmonic anisotropic gold nanorods (AuNRs) have been popularized as orientation probes in single-particle rotational tracking because their shapes induce anisotropic optical properties,[4–6] large scattering and absorption cross-sections,[7] high photostability,[8] and excellent biocompatibility.[9–11]

Using polarization-based in-focus and defocused orientation imaging methods, researchers have determined the 3D orientations of individual AuNRs under dark-field (DF) microscopy,[5,12,13] differential interference contrast (DIC) microscopy,[6,14,15] and total internal reflection scattering (TIRS) microscopy.[16,17] Recently, interference-based DIC microscopy has detected the fast rotational motions of AuNRs with high temporal and spatial resolution in dynamic environments, such as complicated living cells. DIC microscopy is insensitive to the light scattered from the surrounding cellular components and maintains its high-throughput capability in live cell imaging. Sensitivity to scattered light is the main drawback of scattering-based DF and TIRS microscopes.[4,6]

Despite the recent advances in single-particle rotational tracking techniques, depositing and characterizing AuNRs with random 3D orientations on a glass slide on the same focal plane for DIC microscopy is a challenging task. Vertical scanning by the agarose gel-matrix method (or polyvinyl alcohol-matrix method) has characterized the out-of-plane spatial orientations of single AuNRs embedded with random 3D spatial distributions in a gel matrix.[4] However, DIC microscopy can determine only the 3D orientations of the AuNRs on different focal planes as the sample is scanned along the *z*-axis.

In this study, we demonstrate that when deposited on a glass slide, single AuNRs (10 nm × 30 nm) inside a spherical mesoporous silica shell (AuNRs@mSiO$_2$) randomly orient on the same focal plane in 3D space.[11,18] Therefore, DIC microscopy can characterize the random orientations of single AuNRs@mSiO$_2$ with high-throughput on the same focal plane within a single frame. We demonstrate that DIC polarization anisotropy can effectively resolve the azimuthal angle φ of the AuNR cores inside the spherical silica shell. In comparison to

[a]*Department of Chemistry, University of Ulsan, 93 Daehak-ro, Nam-gu, Ulsan 44610, Republic of Korea. E-mail: jwha77@ulsan.ac.kr; Fax: +82 52 712 8002; Tel: +82 52 712 8012*

[b]*Energy Harvest-Storage Research Center (EHSRC), University of Ulsan, 93 Daehak-ro, Nam-gu, Ulsan 44610, Republic of Korea*

[c]*SKKU Advanced Institute of Nanotechnology (SAINT), Research Center for Advanced Materials Technology, Sungkyunkwan University (SKKU), Suwon, 16419, Republic of Korea. E-mail: jhlee7@skku.edu; Fax: +82 502 302 1918; Tel: +82 31 290 7404*

[d]*School of Advanced Materials Science and Engineering, Sungkyunkwan University (SKKU), Suwon, 16419, Republic of Korea*

† Electronic supplementary information (ESI) available: Experimental details, supplementary figures and movie. See DOI: 10.1039/d0ra04704j

the previous work using defocused DF microscopy based on a pattern matching method, DIC microscopy can provide faster and more accurate angular information of spherical AuNRs@mSiO$_2$ without sacrificing the much reduced signal intensity.[18]

Experimental

Materials and chemicals

L-Ascorbic acid, silver nitrate ($AgNO_3$), sodium borohydride ($NaBH_4$), sodium hydroxide (NaOH), 2,6-dihydroxybenzoic acid, tetraethyl orthosilicate (TEOS), gold chloride trihydrate (HAuCl4·3H2O), cetyltrimethylammonium bromide (CTAB) were obtained from Sigma-Aldrich (St Louis, MO, USA). Gold nanorods (AuNRs, 25 nm × 73 nm) were purchased from Nanopartz (Loveland, CO, USA). Deionized water (18.2 MΩ cm) was prepared by a Sartorius Arium®Pro Ultrapure water system. All glassware was cleaned using aqua regia. Special care has to be taken when researchers handle aqua regia.

Characterization of the synthesized AuNRs@mSiO$_2$

We used transmission electron microscope (TEM, JEL-2100F, JEOL, Japan) and scanning electron microscope (SEM, JSM-6500, JEOL, Japan) to characterize the AuNRs@mSiO$_2$. The TEM images were analyzed based on a custom MATLAB script previously reported with some subroutine implemented in the image processing toolbox of MATLAB. Furthermore, a Varian Carry 300 UV-vis spectrometer (Agilent Technologies) was used to characterize the ensemble extinction spectrum of the AuNRs@mSiO$_2$.

Sample preparation for single particle study

The samples for single particles studies were prepared as follows: the colloid solution was first diluted with 18.2 MΩ pure water to a proper concentration. The diluted solution was then sonicated for 10 min at room temperature. Samples were prepared by drop casting the diluted AuNRs@mSiO$_2$ solution on pre-cleaned glass slides. Subsequently, a 22 mm × 22 mm No. 1.5 coverslip (Corning, NY, USA) was placed on the glass slide. Throughout all of the experiments, the concentration of AuNRs@mSiO$_2$ deposited on the glass slide surface was maintained at about 1 μm^{-2} to facilitate single particle characterization without inter-particle interaction and LSPR coupling.

Differential interference contrast microscopy

We performed DIC microscopy using a Nikon inverted microscope (ECLIPSE Ti-U, JAPAN). DIC microscopy consists of a set of two Nomarski prisms, two polarizers, and a quarter-waveplate. We illuminated the samples by an oil immersion condenser with a NA of 1.4. The DIC signals coming from the sample were collected by a Plan Apo oil-immersion objective (100×, NA = 1.4). To obtain DIC images with high quality, we used an Andor EMCCD camera (iXon Ultra 897, UK). We then used Image J and Matlab to analyze the collected DIC images.

Results and discussion

Elliptical and spherical AuNRs@mSiO$_2$ particles were fabricated by a slightly modified literature protocol,[19,20] and were structurally characterized by TEM and SEM. Fig. 1A is a TEM image of the synthesized AuNRs with an average length and diameter of 30 nm and 10 nm, respectively. Elliptical (thin shell) or spherical (thick shell) mesoporous silica was coated on the AuNRs by the above-mentioned modified method (Fig. 1B and C).[19,20] The elliptical mesoporous silica shell was 31.7(±4.8) nm thick, while the spherical mesoporous silica shell was 52.7(±5.7) nm thick (Fig. 1B and C). Additional TEM images showing many nanoparticles are provided in Fig. S1.† We then obtained the UV-vis absorption spectra of the AuNRs and AuNRs@mSiO$_2$ (elliptical and spherical) dispersed in water (Fig. 1D). The longitudinal surface plasmon resonance (LSPR) peaks of the naked AuNRs and the spherical AuNRs@mSiO$_2$ appeared at 769 and 794 nm, respectively. The red shift in the latter LSPR peak was caused by the mesoporous silica shell coating.

Thus far, AuNRs have been randomly oriented in 3D space by embedding them in agarose gel matrix. The 3D orientations must then be determined on successive focal planes by scanning along the *z*-axis (Fig. S2†). However, the gel-matrix method is time consuming, cumbersome, and inconvenient for a 360° rotational study. Furthermore, LSPR coupling can occur among adjacent AuNRs, causing a spectral shift in single-particle characterization.

In our spherical AuNRs@mSiO$_2$ fabrication, LSPR coupling between two adjacent AuNRs is prevented by the outer shell, which is advantageous for single-particle spectroscopic

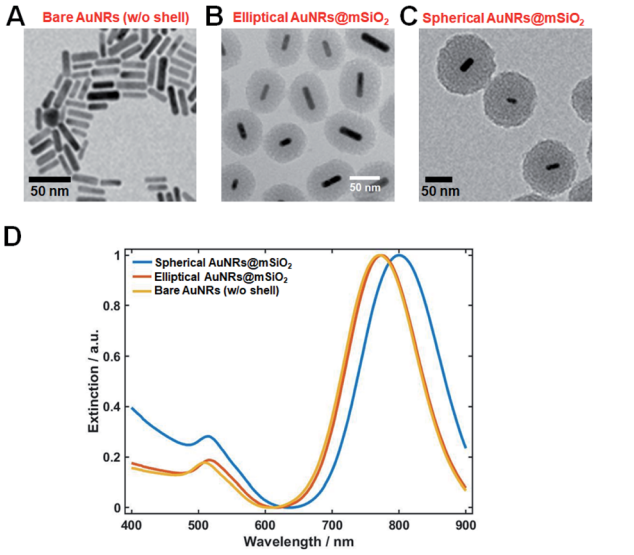

Fig. 1 (A–C) TEM images of (A) bare AuNRs, (B) elliptical AuNRs@mSiO$_2$ (red curve), and (C) spherical AuNRs@mSiO$_2$ (blue curve). (D) Overlaid UV-vis extinction spectra of bare AuNRs (yellow curve), elliptical AuNRs@mSiO$_2$ (red curve), and spherical AuNRs@mSiO$_2$ (blue curve). The anisotropic AuNRs yielded two distinct LSPR peaks.

characterization (Fig. 1C and S1C†). However, the silica shell can block the interaction of AuNRs with the medium. Furthermore, during the drop-casting for sample preparation, the naked AuNRs were deposited parallel to the glass slide, so were tilted by almost the same angle from the glass surface (see Fig. 2A). The elliptical AuNRs@mSiO$_2$ with the thin silica shell were also tilted at very similar angles, with low degrees of freedom in the *z*-direction (Fig. 2B). In contrast, within the silica shells of the spherical AuNRs@mSiO$_2$ deposited on the glass slide, the AuNR cores were randomly oriented on the same focal plane (Fig. 2C), with different projected lengths. As shown in Fig. 1C and 3A, the 3D orientations of the AuNRs in the shells influenced the projected lengths of the AuNRs. This situation completely differed from that of bare AuNRs (Fig. 1A and S1A†). The random 3D orientations of many AuNRs in the silica shell was further verified by SEM (see Fig. 3B and S3†).

We then investigated the spatial orientations of single AuNR (10 nm × 30 nm) cores in the silica shell by DIC microscopy. The experimental setup of the single-particle microscopy and spectroscopy is presented in Fig. S4.† As an interferometry-based technique, DIC microscopy resolves the optical path difference between two orthogonally polarized beams (B1 and B2, designating the bright and dark axes, respectively) separated by a Nomarski prism (Fig. S5†). The azimuthal angle (φ) and polar angle (θ) of the AuNR core are defined in Fig. S6.† The DIC captured single spherical AuNRs@mSiO$_2$ particles in the same focal plane at their LSPR wavelength (*i.e.*, at 750 nm) (Fig. 3C). It should be noted that in DIC microscopy, the different bright and dark patterns correspond to different in-plane orientations of the AuNR cores deposited on the glass slide. Therefore, we could achieve high-throughput, high-contrast DIC imaging of spherical AuNRs@mSiO$_2$ particles with various orientations within a single image frame.

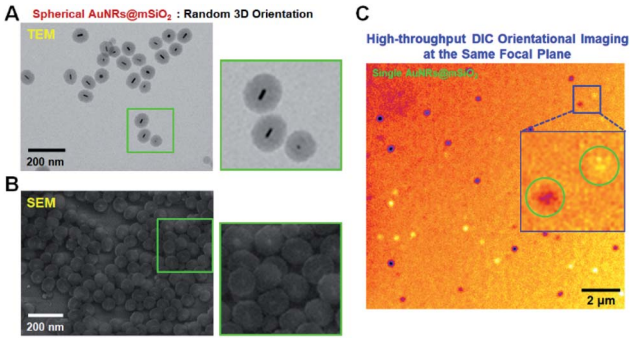

Fig. 3 (A) TEM image of spherical AuNRs@mSiO$_2$ with randomly oriented AuNR cores inside the silica shell. (B) SEM image of spherical AuNRs@mSiO$_2$ particles, and (C) DIC image of AuNRs@mSiO$_2$ particles, showing their different orientations on the same focal plane. The color image was generated in ImageJ for better demonstration of bright and dark DIC images of AuNRs@mSiO$_2$. Note that high-throughput detection is possible.

The polarization dependency of the spherical AuNRs@mSiO$_2$ imaging was measured at their LSPR wavelength (750 nm) on a rotational stage moved from 0° to 360° at 10° increments. Fig. 4A is a DIC image of two spherical AuNRs@mSiO$_2$ particles (labelled AuNR1@mSiO$_2$ and AuNR2@mSiO$_2$) measured at 750 nm. As shown in Fig. 4B and S7,† the DIC images of AuNR1@mSiO$_2$ periodically changed as the rotation angle increased. The polarization dependency of

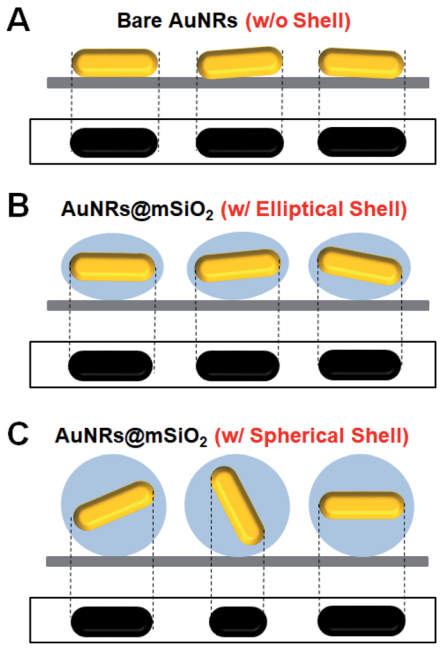

Fig. 2 (A) Schematic of bare AuNRs deposited on a glass slide. Their projected lengths are almost the same. (B) Schematic of elliptical AuNRs@mSiO$_2$ particles and their projections on a glass slide. (C) Schematic of spherical AuNRs@mSiO$_2$ particles with their AuNR cores randomly oriented in the shell. Their projected lengths depend on their spatial orientations, which are freely available in 3D space.

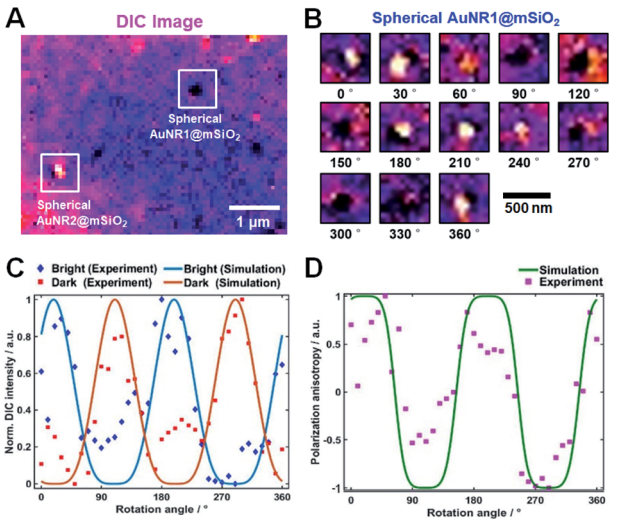

Fig. 4 (A) DIC image of spherical AuNRs@mSiO$_2$. (B) DIC images of spherical AuNR1@mSiO$_2$ captured at different rotational angles (interval = 30°). (C) Dark and bright intensities of spherical AuNR1@mSiO$_2$ as functions of rotation angle. (D) DIC polarization anisotropy computed from the dark and bright intensities of the spherical AuNR1@mSiO$_2$.

the DIC images was further confirmed in AuNR2@mSiO$_2$ (Fig. S8†). In addition, the bright and dark intensities of AuNR1@mSiO$_2$ were periodic functions of rotation angle and were anti-correlated at both LSPR wavelengths (769 and 794 nm), informing that when the dark intensity decreases, the bright intensity increases (Fig. 4C). In this study, the measured dark and bright values consist of the darkest and brightest pixels within a region around a particle, respectively. The bright and dark intensities at each LSPR wavelength were well fitted to $\sin^4(\varphi)$ and $\cos^4(\varphi)$ functions, respectively. More specifically, the orthogonally polarized bright and dark intensities of AuNR@mSiO$_2$ are given by[12,18]

$$I_B \propto \sin^4(\phi)\sin^2(\theta)$$
$$I_D \propto \cos^4(\phi)\cos^2(\theta) \quad (1)$$

According to eqn (1), the AuNR orientations are directly determinable from the bright and dark intensities of the polarized DIC images. In practice, however, the precision might be affected by intensity fluctuations of the light source, focus-drift in the vertical direction, and other disturbances. This limitation can be overcome by the DIC polarization anisotropy P, defined by eqn (2).[6,14] The DIC polarization anisotropy P can be conveniently computed from the bright and dark intensities of AuNR@mSiO$_2$:

$$P = \frac{I_{B,N} - I_{D,N}}{I_{B,N} + I_{D,N}} \quad (2)$$

Here, $I_{B,N}$ and $I_{D,N}$ are the normalized bright and dark intensities at the LSPR wavelengths, respectively. As the polarization direction increased from 0° to 360°, the DIC polarization anisotropy of the AuNR1@mSiO$_2$ varied between −1.0 (AuNRs alignment along the dark axis, $\varphi = 0°$ or 180°) and 1.0 (AuNR alignment along the bright axis, $\varphi = 90°$ or 270°) (see Fig. 4D). Being based on the intensity ratio rather than the absolute intensities, the DIC polarization anisotropy is resistant to intensity instabilities and provides reliable and accurate angle measurements.[14] Moreover, the DIC polarization anisotropy depends only on the azimuthal angle φ, and not on the polar angle θ of the AuNRs.[6] After determining the azimuthal angle φ of AuNRs@mSiO$_2$ by DIC polarization anisotropy, we can determine their polar angles θ by eqn (1).

Next, we compared the polarization angles of the spherical AuNRs@mSiO$_2$ and the elliptical AuNRs@mSiO$_2$ with the thin silica shell. The polarization angles of the elliptical AuNRs@mSiO$_2$ particles were measured at their LSPR wavelength (750 nm) on a rotational stage shifted at 10° increments from 0° to 360°. Fig. S9† shows the DIC images of the elliptical AuNR1@mSiO$_2$ measured at their LSPR wavelength at different rotation angles. Again, the bright and dark intensities of the elliptical AuNR1@mSiO$_2$ were periodic functions of rotational angle (Fig. S10A†), and the measured DIC polarization anisotropy values well agreed with the calculated values (Fig. S10B†). After determining the azimuthal angle φ of the elliptical AuNRs@mSiO$_2$ by DIC polarization anisotropy, we determined their polar angles θ. As shown in Fig. 5A, the polar angles θ of the AuNR cores inside the elliptical silica shell varied between 60° and 90°. In addition, the polar angles θ of bare AuNRs without the shell also varied between 60° and 90° (Fig. S11†). However, the AuNR cores inside the spherical silica shells were distributed over a wider range (0–90°, see Fig. 5B) because more degrees of freedom, especially in the vertical direction, were available to the AuNRs in the spherical shells.

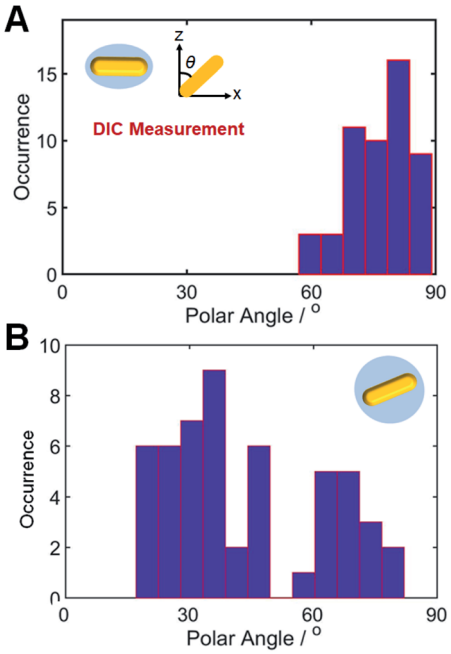

Fig. 5 Histograms showing the polar angle (θ) distributions of (A) elliptical AuNRs@mSiO$_2$ and (B) spherical AuNRs@mSiO$_2$, determined from the DIC measurements.

Finally, to clearly demonstrate the advantage of the spherical AuNRs@mSiO$_2$ fabrication over the conventional gel-matrix method, we imaged tilted AuNRs (of average size 25 nm × 73 nm) embedded in a 2% agarose gel matrix. DIC images of AuNRs were obtained by scanning along the z-direction with a vertical step size of 40 nm (Movie S1†). Fig. S12† shows consecutive DIC images of the AuNRs with random 3D orientations in the gel matrix, obtained on different focal planes. The different focal planes of the AuNRs in the gel matrix are clarified in Fig. S12.† This result confirms that without vertical scanning, DIC microscopy cannot observe the random spatial orientations of the AuNRs in the standard gel-matrix embedding. In contrast, the spherical AuNRs@mSiO$_2$ enables a high-throughput determination of the 3D orientations of the AuNR cores in the silica shell on a single focal plane of the objective; moreover, it prevents LSPR coupling among the nanoparticles.

Conclusions

In summary, the spatial orientations of single AuNRs (10 nm × 30 nm) coated with mesoporous silica shell (AuNRs@mSiO$_2$) were observed by DIC microscopy. The silica shell prevented LSPR coupling among the AuNR cores. Unlike the bare AuNRs and elliptical AuNRs@mSiO$_2$, spherical AuNRs@mSiO$_2$ deposited on a glass slide allowed random 3D orientations of the

AuNR cores on the same focal plane. These orientations were detected with high-throughput and high-contrast efficacy within a single frame. Our approach newly characterizes the 3D random orientations and polarization dependences of AuNRs on the same focal plane by DIC microscopy. The main limitation of the gel-matrix method, namely, the need for observing many focal planes along the *z*-direction, is thereby removed.

Conflicts of interest

There are no conflicts to declare.

Acknowledgements

This work was supported by a National Research Foundation of Korea (NRF) grant funded by the Korean government (MSIP) (No. 2018R1C1B3001154) and the grant for Bio-inspired Innovation Technology Development Project (NRF-2018M3C1B7021997) funded by the Ministry of Science and ICT. This work was also supported by a National Research Foundation of Korea (NRF) grant funded by the Korean government (MSIP) (No. 2019R1A6A1A11053838).

Notes and references

1 X. Zhuang, L. E. Bartley, H. P. Babcock, R. Russell, T. Ha, D. Herschlag and S. Chu, *Science*, 2000, **288**, 2048–2051.
2 T. Nishizaka, K. Oiwa, H. Noji, S. Kimura, E. Muneyuki, M. Yoshida and K. Kinosita, *Nat. Struct. Mol. Biol.*, 2004, **11**, 142–148.
3 E. Toprak, J. Enderlein, S. Syed, S. A. McKinney, R. G. Petschek, T. Ha, Y. E. Goldman and P. R. Selvin, *Proc. Natl. Acad. Sci. U. S. A.*, 2006, **103**, 6495–6499.
4 L. Xiao, J. W. Ha, L. Wei, G. Wang and N. Fang, *Angew. Chem., Int. Ed.*, 2012, **51**, 7734–7738.
5 C. Sönnichsen and A. P. Alivisatos, *Nano Lett.*, 2005, **5**, 301–304.
6 J. W. Ha, W. Sun, A. S. Stender and N. Fang, *J. Phys. Chem. C*, 2012, **116**, 2766–2771.
7 S. Link and M. A. El-Sayed, *Annu. Rev. Phys. Chem.*, 2003, **54**, 331–366.
8 W.-S. Chang, J. W. Ha, L. S. Slaughter and S. Link, *Proc. Natl. Acad. Sci. U. S. A.*, 2010, **107**, 2781–2786.
9 C. J. Murphy, A. M. Gole, J. W. Stone, P. N. Sisco, A. M. Alkilany, E. C. Goldsmith and S. C. Baxter, *Acc. Chem. Res.*, 2008, **41**, 1721–1730.
10 S. Yoon, J. Chang, N. Kwon, S. Moon, Y. Park, K. H. Han, B. Lim and J. H. Lee, *BioChip J.*, 2019, **13**, 236–242.
11 S. Yoon, Y. Chung, J. W. Lee, J. Chang, J. G. Han and J. H. Lee, *BioChip J.*, 2019, **13**, 362–369.
12 L. Xiao, Y. Qiao, Y. He and E. S. Yeung, *Anal. Chem.*, 2010, **82**, 5268–5274.
13 S. Y. Lee, P. V. Tsalu, G. W. Kim, M. J. Seo, J. W. Hong and J. W. Ha, *Nano Lett.*, 2019, **19**, 2568–2574.
14 J. W. Ha, W. Sun, G. Wang and N. Fang, *Chem. Commun.*, 2011, **47**, 7743–7745.
15 S. Y. Lee, Y. Han, J. W. Hong and J. W. Ha, *Nanoscale*, 2017, **9**, 12060–12067.
16 J. W. Ha, K. Marchuk and N. Fang, *Nano Lett.*, 2012, **12**, 4282–4288.
17 K. Marchuk and N. Fang, *Nano Lett.*, 2013, **13**, 5414–5419.
18 G. W. Kim, S. Yoon, J. Lee, J. H. Lee and J. W. Ha, *J. Phys. Chem. C*, 2020, **124**, 14279–14286.
19 S. Yoon, B. Lee, C. Kim and J. H. Lee, *Cryst. Growth Des.*, 2018, **18**, 4731–4736.
20 I. Gorelikov and N. Matsuura, *Nano Lett.*, 2008, **8**, 369–373.

